Effects of Cyclic Loading Rate on Response f Reinforced Concrete Structures§

철근콘크리트 구조물에 대한 반복하중속도의 영향에 관한 연구

鄭　鑾*
Chung, Lan
박　현　수**
Park, Hyun Soo

요　약

본 논문의 내용은 철근콘크리트 보-기둥 접합부가 지진 하중을 받을때의 거동에 대하여 관찰한 것이다. 똑같이 제작된 두개의 시험체에 정적 반복하중과 동적반복하중을 가하여 하중-처짐 곡선이나 파괴 성상등에 관하여 차이점을 기록하였다. 동적하중을 받는 시험체의 거동은 내진설계 규준에서일반적으로 쓰여지는 정적 하중 하에서의 시험체의 거동과는 판이한 양상을 보여주었다.

시험체가 동적 하중을 받을때에는 정적하중을 받을때 보다

① 극한하중이 20-25%증가하고
② 높은 취성을 보이며
③ 균열이 집중되고,
④ 휨파괴 보다는 전단파괴현상을 나타내었다.

Abstract

Small-scale models of reinforced concrete beam-column joints and anchorage-bond specimens were subjected to large cyclic displacements at two rates. To assess damage, free vibration tests were conducted. The reliability of the modeling techniques was established by comparison of the results for the slower rate with those obtained from the full-scale tests on prototype. The higher rate of loading caused a greater damage than that at the slower rate. This was evidenced by the measurements of the stiffness obtained from the free-vibration test. The relatively greater extent of damage appears to result from the different bond behavior at different rates of loading.

1. INTRODUCTION

The current practice for design of reinforced concrete structures subjected to earthquake loading is based primarily on the experimental results of structural elements and assemblages subjected to cyclic loading at the quasi-static loading rates [1, 2]. These rates are substantially lower than those corresponding to the frequencies of seismic

* 정회원, 단국대 건축공학과 부교수, 공박
§ 본 연구는 1988년도 한국과학재단의 신진연구비의 지원에 의한 것임.

□ 이 논문에 대한 토론을 1989년 12월 31일까지 본학회에 보내주시면 1990년 6월호에 그 결과를 게재하겠습니다.

excitation. A few studies which have been conducted to ascertain the influence of dynamic rates of loading present somewhat conflicting evidence [3, 4].

In this study, small-scale model reinforced concrete beam-column joints and anchorage-bond specimens were subjected to cyclic loading at two different rates. The reliability of the modeling techniques was established by comparing the results of the test at the slower rate with those of the full-scale tests conducted by previous investigators[5, 6, 7]. Several different parameters were examined to evaluate the differences due to the rate of loading.

BEAM-COLUMN JOINT SPECIMENS

Test Specimen

Three identical beam-column joints (Fig. 1) were fabricated. The first specimen was for the preliminary test to determine the yield displacement and to check the instrumentation. The second specimen was subjected to cyclic loading at the frequency of 2.5 x 10^{-3} Hz(slow rate) while the third specimen was tested at the frequency of 1.0 Hz(fast rate). The details of column design, beam design and joint design are given in Table 1.

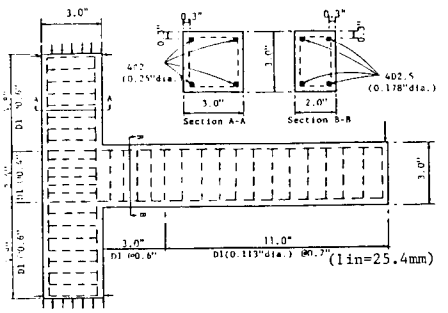

Fig. 1 Model beam-column joint specimen design

Specimens were horizontally cast in waterproofed plywood forms. Reinforcing steel cages were assembled according to the applicable specifications of the ACI Building Code [8]. Stirrups in the joint were fabricated as per ACI-ASCE Joint Committee 352 Recommendations [9]. They were tied by 20-gage annealed wires (D=0.0320″) to the longitudinal reinforcement. A dimensional tolerance of less than 5% was achieved in the construction of the specimens.

Concrete was compacted with an electric vibrator. Specimens and cylinders were tested after 28 days of curing in a 96% relative humidity and 80°F environment

Material Properties

The properties of the three types of steel rein-

Table 1a. Comparison of column design between model and prototype

	(in) size (B×D)	(in) column length	main size(in²)	steel ratio(%)	tie bar	(psi) shear stress $v_u=Vu/\phi bd$	(psi) allowebie v_c	(in) tie space required	(in) tie space used
P	8×12	60.	4#6(1.76)	2.20	#2	239.0	155.0	6.0	2.25
M	3×3	12.	4#2(0.20)	2.50	D1	181.5	184.0	8.4	0.60

Table 1b. Comparison of beam design between model and prototype

	(in) size (b×l)	(in) column length	(in²) main steel size top	(in²) main steel size bott.	ratio(%) top	ratio(%) bott.	(in²) stirrup	(kips) max. beam shear force calculated	(kips) max. beam shear force measured
P	8×10	31.0	2#6(0.98)	2#5(0.72)	1.23	1.0	#2(0.05)	16.9	15.2
M	2×3	13.5	2D2.5(.05)	2D2.5(.05)	0.84	0.9	D1(.0083)	0.776	0.725

	max.beam shear stress (in)		allowable (in)	tie space (in)	max. (in)	tie space (in)
	calculated	measured	v_c	required	(d/4)	used
P	247.0	221.0	129.0	4.13	2.0	2.0
M	169.0	158.0	126.0	7.7	0.675	0.6

(lin=25.4mm, 1kip=4448N, 1ksi=6895kpa)
P=prototype
M=model

Table 1c. Comparison of joint design between model and prototype

	core (in) size	tie (in) bar	joint shear force (kips) $V_j = T_s - V_{u\,col}$	joint shear stress (ksi) $v_j = V_j / \phi bd$	allowable (ksi) v_c	tie bar spacing (in) required	used
P	7.×8.6×9.64	#2(.05)	67.5	1.18	0.306	2.2	1.75
M	1.4×2.4×2.4	D1(.0083)	3.38	0.74	0.371	0.91	.4

forcement used for beam (D2.5 bar) and column longitudinal reinforcement (#2 bar) and for shear reinforcement (D1 bar) are given in Table 2.

Mix proportions of concrete are also given in Table 2. Three 3″ x 6″ cylinders were cast and cured simultaneously with each specimen and subjected to uniaxial compressive loading on the same day the beam-column subassembly was tested. Average modulus of elasticity (secant at 0.45 f_c') was 3.0 x 10^6 psi and the average compressive strength was 4000 psi.

Loading Procedure

A reaction frame was built around the specimen-column to transfer the loads to the MTS supporting steel columns (Fig. 2). The specimen-column was subjected to a 8.0 kips applied frame load during the testing. This load was approximately 50% of the balanced design load of the column.

After a predetermined loading history, the cyclic loading was interrupted and free vibration tests were conducted. A displacement corresponding to the 10% of the yield displacement was imposed by the loading ram. This displacement was allowed to dampen out by suddenly cutting the wire connecting the beam-end at the loading ram.

The loading schedule imposed at two different rates on the two specimens is shown in Fig. 3. The displacement ductility ratio is defined here as the ratio of the displacement of the beam at the load-point at any stage in testing to the corresponding displacement at the initial yield of the beam longitudinal steel under positive shear.

Table 2. Comparison of material properties between model and prototype

* not measured
** not reported

Reinforcement　(1 ksi=6895 kpa)

Specimen	Type	No. of bar	f_y (ksi)	$\varepsilon_y (\times 10^{-3})$	E_s(ksi)	σ_{max}(ksi)
Model	Beam-column joint and anchorage-bond specimen	D2.5	85	3.2	28800	93.0
		#2	68	2.4	28000	*
		D1	40	1.7	23500	*
Prototype	Beam-column joint specimen	#6	52.7	2.0	28200	84.8
		#2	42.6	*	*	*
	Anch.-bond specimen	#6	45	1.55	29000	79.0

Concrete

Specimen	Test cylinder	f_c'(ksi)	Max. aggregate	Mix proportions(wt)		
				cement	aggregate	water
Model	3−3″×6″	4.0	3/16″	1.0	4.0	0.59
Beam-col prototype	3−4″×8″	4.0	3/8″	1.0	6.1	0.50
Anch.-bond prototype	6″×12″	5.3	3/4″	**	**	**

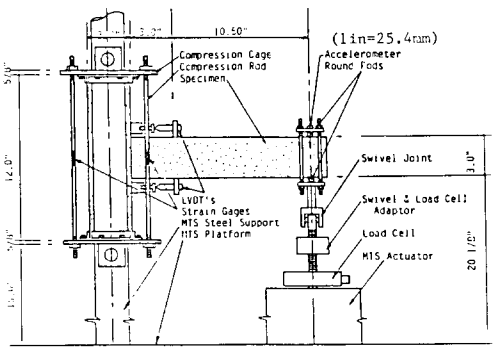

Fig. 2 Sideview of beam−column joint specimen test set−up

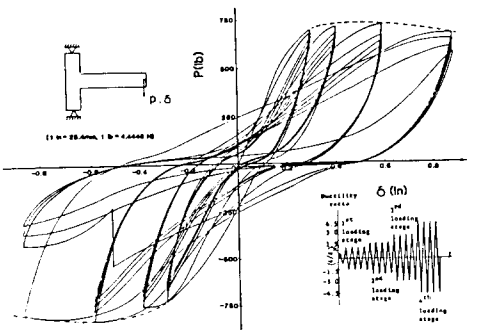

Fig. 3 Load−deflection diagram for beam−column joint specimen($f=2.5\times10^{-3}$ Hz)

The yield load and corresponding displacement as measured during the preliminary test were approximately 650 lbs and 0.2 in., respectively.

The instrumentation was designed to monitor the behavior of the specimens during the test by providing a continous time record of applied load, displacements and acceleration. The load was measured by a LEBOW Model 3157 load−cell attached to the MTS actuator (Fig. 2) while the acceleration during free vibration test was measured by an Endevco Model 7265−A−HS accelerometer attached to the tip of the beam. To measure the average rotation of beam hinging region, two linear variable differential transformers (Schaevitz Model 500 MHR LVDT) were positioned on the top and bottom of the beam near the column. They measured displaccements over a gage length equal to the depth of the beam. The analog signals from the various measuring devices were conditioned, amplified, and digitized

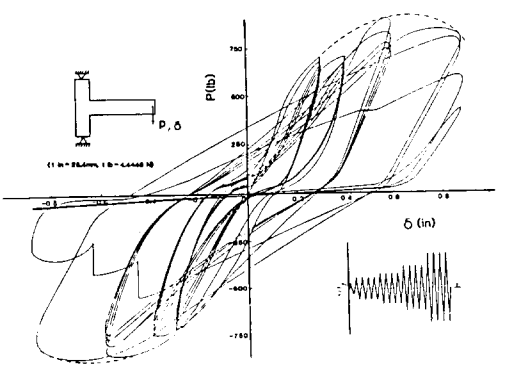

Fig. 4 Load−deflection diagram for beam−column joint specimen(f=1.0 Hz)

using an A/D converter and then recorded in a computer based storage system (ISAAC 2000) The real time load vs actuator displacement was also recorded on an X−Y plotter.

Test Results

The load−deflection hysteresis curves as measured

by the x−y plotter are shown in Fig. 3 for the slow rate test and in Fig. 4 for the fast rate loading test. From these two sets of curves and corresponding cyclic envelope curves shown in Figs. 3 and 4 it can be seen that the maximum load carrying capacity of the specimen is somewhat higher at the higher rate of loading. However, the damage induced by the cyclic loading seems to be higher for the faster rate of loading. This is evidenced in the sharper drop after the peak of the envelope curve for the faster rate of loading. The relatively greater extent of damage caused by the fast rate of loading was also evidenced by the results of the free vibration tests shown in Fig. 5.

During the 4th loading stage, one of the top steels of the beam fractured during the second negative cycle for the slow rate test. For the specimen tested at the faster rate of loading, all the top steel fractured during the same loading cycle.

Developments of major cracking in the model were also observed. It can be seen in Fig. 6a for the slow rate test and in Fig. 6b for the fast rate test.

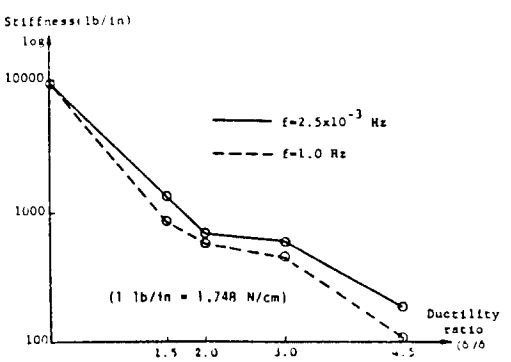

Fig. 5 Stiffness degradation measured from beam−column joint

Comparison with a Prototype

In order to evaluate the validity of testing small−scale models, the results of the specimen No. 6 tested by Scribner and Wight [5]. The dimensions of their specimen and the design of

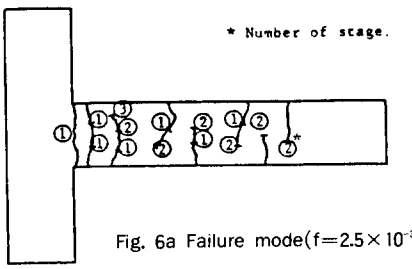

Fig. 6a Failure mode($f=2.5\times10^{-3}$ Hz)

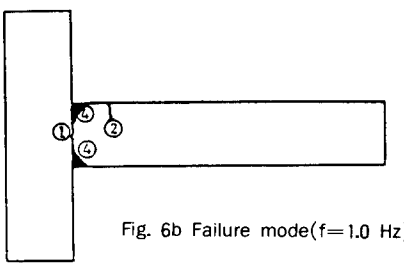

Fig. 6b Failure mode($f=1.0$ Hz)

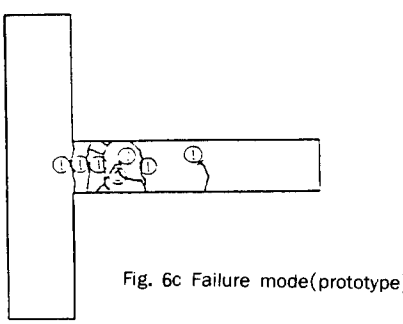

Fig. 6c Failure mode(prototype)

their column, beam and beam−column joint are compared with the model specimen in Table 1.

The cyclic envelope curve obtained from the results of the specimen tested by Scribner and Wight is compared with the one obtained from the present investigation in Fig. 7. For comparison purposes the model loads and deflections were normalized according to the similitude requirements.

Development of major cracking in the model was also observed to be similar to that for the prototype (Fig. 6c). The regions of the columns away from the joint showed no cracking or degradation. Both beams showed primarily flexural cracks as can be seen in Figs. 6a and 6c.

ANCHORAGE BOND TEST

By comparing crack patterns reproduced in Fig. 6a and 6b, it was observed that flexural cracks were widely distributed for the specimen tested at the slow rate. In contrast, for the fast rate, the damage was essentially due to a single wide crack observed at the face of the column. This indicates that the observed rate effect may be related to the transfer of forces between reinforcing bars and concrete.

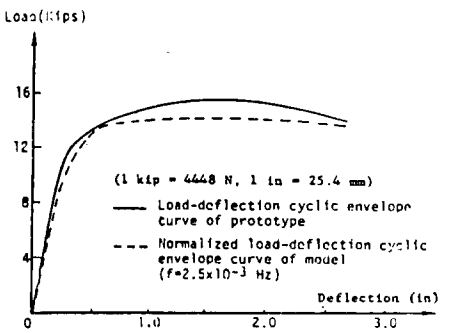

Fig. 7 Comparison of load-deflection curve between prototype and model(beam-colunm joint)

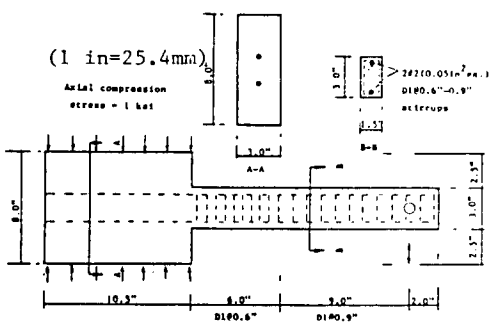

Fig. 8 Model anchorage-bond specimen design

Loading Procedure

A structural framework was required around the MTS supporting steel columns to act as a reaction frame. The enlarged block of the specimen was subjected to a 1 ksi applied compression stress to simulate a column during the testing. The complete sideview of this test set-up is shown in Fig. 9.

The loading schedule imposed at two different rates(2.5×10^{-3} Hz and 0.5 Hz) on the two specimens is shown in Fig. 10. At the higher rate, the expected

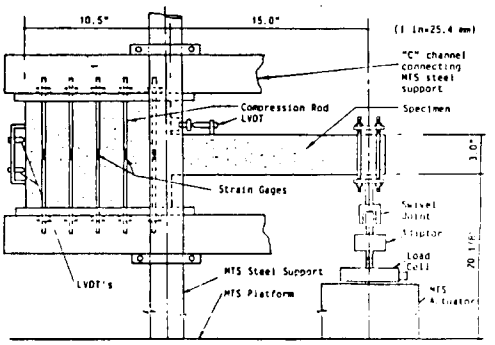

Fig. 9 Sideview of anchorage-bond specimen test set-up

displacements were not reached due to the mechanical limit of the testing machine. The maximum amplitude was about 80% of the expected value at each stage.

In addition to the instruments used in beam-column joint specimen tests, two more LVDTs were positioned on the end of the reinforcements inside the enlarged end block. They measured the end slip of the longitudinal reinforcements.

Test Results

Load-deflection curves of two specimens are shown in Fig. 10 for the slow rate test and in Fig. 11 for the fast rate test. The ultimate load of fast rate test was higher(about 25%) than that of slow rate test. This result is similar to that beam-column joint specimen test result.

Although the expected displacements were not reached for the fast rate test, the failure of test specimen occurred after about the same number of cycles as that for the slow-rate test. This indicates that the specimen subjected to fast rate of loading can sustain a smaller magnitude of

cyclic excursion than the specimen subjected to slow rate of loading.

Failure modes compared in Fig. 12 were also observed to be similar to that for the previous beam-column joint specimens. Flexural cracks were more concentrated and developed more rapidly

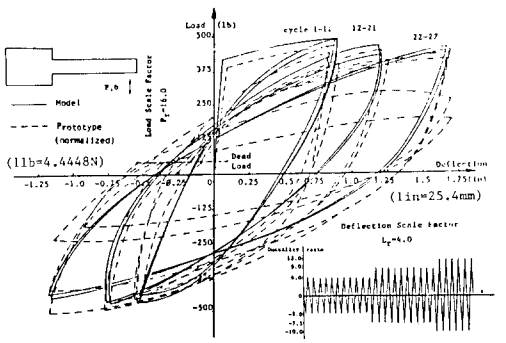

Fig. 10 Load-deflection diagram for anchorage-bond specimen (f=2.5× 10 ^{3} Hz)

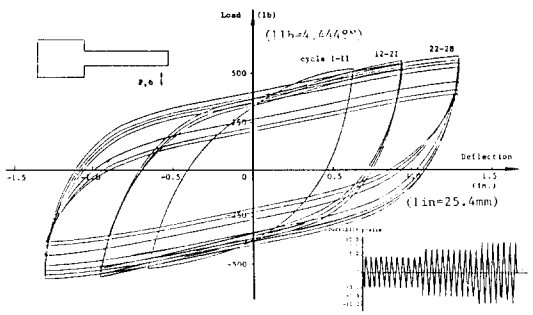

Fig. 11 Load-deflection diagram for anchorage-bond specimen (f=0.5 Hz)

for the fast rate test than for the slow rate test.

No end slips were observed at the fast rate test during testing. On the other hand, 0.0005″ ~0.0006″ of end slip were observed at the last stage (cycle 22-27) for the slow rate test specimen. This indicates that the bond stresses were transferred to the end of the embedded longitudinal reinforcement more effectively for the slow rate test than for the fast rate.

Comparison with a Prototype

The results of the specimen tested at the slow rate were compared with specimen 66-32-RV5-60 tested by Brown, Ismail and Jirsa [6, 7]. The material properties of prototype are shown in Table 2. The dimensions of prototype are four times to that of model (L_r=4.0). The section area of longitudinal reinforcement is approximately square of length scale factor ($A_r \simeq L_r^2 = 16.0$).

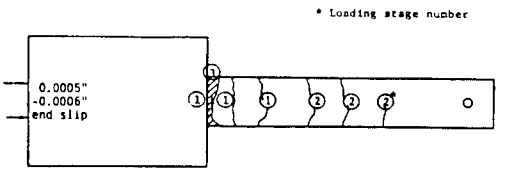

Fig. 12a Failure mode(f=2.5× 10^{-3} Hz)

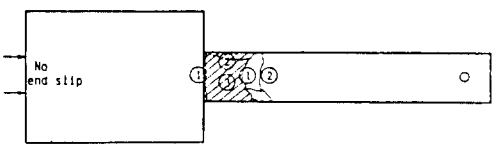

Fig. 12b Failure mode(f=0.5 Hz)

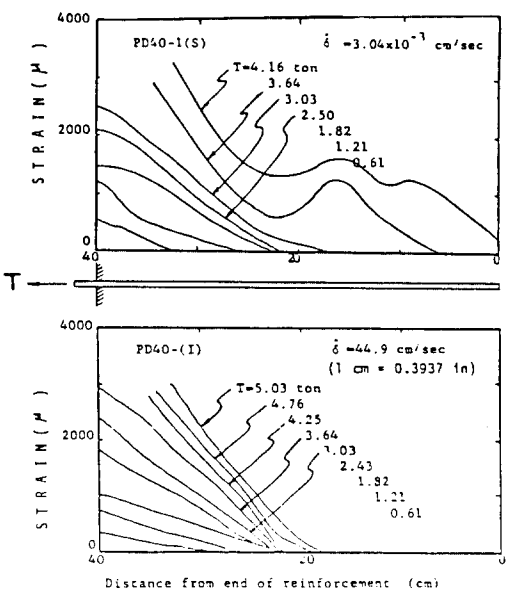

Fig. 13 Comparison of bond stress distribusion on reinforcement between static and high rate Loading test (from ref. 10)

The cyclic curve obtained form the results of the prototype specimen is compared with the one obtained from the model slow rate test in Fig. 10. For comparison purposes the prototype loads and deflections were normalized according to the similitude requirements.

CONCLUSIONS

From the load-derlection curves reported in Figs. 3, 4, 10 and 11 it was observed that the ultimate load for the specimen subjected to fast rate was about 20-25% higher than that for the slow rate but the degradation during the cyclic loading was greater for the fast rate. This was also evidenced from the results of the free vibration tests reported in Fig. 5.

By comparing crack patterns and end slips of longitudinal reinforcement it was observed that flexural cracks were widely distributed and 0.0005″- 0.0006″ end slips were obtained for the specimen tested at the slow rate. In contrast, the damage was due to a single wide crack observed at the face of the column and no end slips were obtained for the fast rate test specimen. This indicates that the observed rate effect is essentially related to the transfer of forces between reinforcing bars and concrete. It is likely that the first flexural crack in the beam developed at the face of the column for both specimens. However, because of the more efficient load-transfer occurring at the slow rate, additional cracking progressively developed at sections further away from the column face. Some support for such an argument can be obtained from the results reported by Takeda [10]. He studied the rate effect on the bond stress distribution on deformed bar during a pull-out test. Some of his results are shown in Fig. 13. The bond stress distribution at two different rates are shown. It can be seen that bond stresses are more localized at the higher rate.

REFERENCES

1. Hawkins, N. M., Editor, "Reinforced Concrete Structures in Seismic Zones," *ACI-Publication*, SP-53, pp.485, 1977.
2. Wight, J. K., Editor, "Earthquake Effects on Reinforced Concrete Structures," *ACI-Publication*, SP-84, pp.428, 1985.
3. Mutsuyoshi, H. and Machida, A., "Dynamic Properties of Reinforced Concrete Piers," *Transactions of the Japan Concrete Institute*, Vol. 4, pp.424-436, 1987.
4. Wilby, G. K., "Response of Concrete Structures to Seismic Motions," Ph. D. thesis, Department of Civil Engineering, University of Canterbury, New Zealand, pp. 225, 1976.
5. Scribner, C. F., and Wight, J. K., "Delaying Shear Strength Decay in Reinforced Concrete Load Reversals", Department of Civil Engineering, University of Michigan, pp. 220, May 1984.
6. Ismail, M., "Bond Deterioration in Reinforced Concrete Under Cyclic Loading," Ph. D. Thesis, Rice University, Houston, Texas, pp. 164, March 1970.
7. Brown, R. H., "Reinforced Concrete Cantilever Beams under Slow Cyclic Loadings," Ph. D. Thesis, Rice University, Houston, Texas, pp. 166, April 1970.
8. ACI Committee 318, "Building Code Requirements for Reinforced Concrete (ACI 318-83)," American Concrete Institute, Detroit, pp. 111, 1983.
9. ACI-ASCE Joint Committee 352, "Recommendations for Design of Beam-Column Joints in Monolithic Reinforced Concrete Structures", *ACI Journal*, pp. 375-393, July 1976.
10. Takeda, J. I., "Dynamic Fracture of Concrete Structures Due to Severe Earthquakes and Some Consideration on Countermeasures", *8th World Conference on Earthquake Engineering*, Vol. VI, San Francisco, pp. 299-306. 1984.

(접수일자 : 1989. 7. 10